Nanoscale

Hexagonal Layered Group IV-VI Semiconductors and Derivatives: Fresh Blood of 2D Family

Journal:	*Nanoscale*
Manuscript ID	NR-ART-03-2020-002217.R1
Article Type:	Paper
Date Submitted by the Author:	17-May-2020
Complete List of Authors:	Tian, Xiaoqing; ShenZhen University, Physics Duan, Yijing; Shenzhen University Kiani, Maryam; Sichuan University, Wei, Yadong; Shenzhen University, Physics Feng, Naixing; Shenzhen University Gong, Zhirui; Shenzhen University, College of Physics and Energy Du, Yu; College of Physics Science and Technology, Wang, Xiangrong; Hong Kong University of Science and Technology Yakobson, Boris; Rice University,

Hexagonal Layered Group IV-VI Semiconductors and Derivatives: Fresh Blood of 2D Family

Xiao-Qing Tian,[ac] Jing-Yi Duan,[a] Maryam Kiani,[a] Ya-Dong Wei,[a] Naixing Feng,[b] Zhi-Rui Gong,[a] Xiang-Rong Wang,*[c] Yu Du,*[a] and Boris I. Yakobson*[d]

[a]*College of Physics and Optical Engineering, Shenzhen University, Shenzhen 518060, Guangdong, P. R. China.*

[b]*College of Electronic Sciences and Technology, Shenzhen University, Shenzhen 518060, Guangdong, P. R. China.*

[c]*Department of Physics, The Hong Kong University of Science and Technology, Clear Water Bay, Kowloon, Hong Kong.*

[d]*Department of Materials Science and NanoEngineering, Department of Chemistry, and the Smalley Institute for Nanoscale Science and Technology, Rice University, Houston, Texas 77005,United States.*

New phases of group IV-VI Semiconductors in the 2D hexagonal structures are predicted and the unusual physical properties are revealed. The structures of monolayer group IV-VI Semiconductors are similar to blue phosphorene and each unit has the same ten valence electrons. The band gap of 2D hexagonal group IV-VI semiconductors depends on both the thickness and stacking order. Atomic functionalization can induce ferromagnetism and the Curie temperature can be tuned. Gapped Dirac Fermions with zero mass are developed and this makes it exceed that of graphene. The Fermi velocity can be compared to or even above that of graphene.

Corresponding authors.

E-mails: phxwan@ust.hk; duyu@szu.edu.cn; biy@rice.edu.

Phones: +852 23587488; +86 (755) 26530931; 713-348-6383.

Faxes: +852 23581652; +86 (755) 26538735; 713-348-5423.

Introduction

Two-dimensional layered materials such as graphene, MoS_2, In_2Se_2, stanene, $Cr_2Ge_2Te_6$ and CrI_3 have exhibited rich and unconventional physics such as Dirac fermions, valley Hall effects, topological insulator state, intrinsic ferromagnetism and giant tunneling magnetoresistance.[1-12] Different from other 2D materials, black phosphorene (BP) is a mono-elemental semiconductor, and it was predicted to have an ultrahigh mobility up to 26000 $cm^2V^{-1}s^{-1}$. BP has received tremendous research attention since the BP field effect transistors were fabricated.[13-16] Blue phosphorene, an allotrope of BP, has been recently synthesized in the experiments and it is an indirect band gap semiconductor with the stability comparable to black phosphorene.[17-21] Two-dimensional III-VI chalcogenides semiconductors have high carrier mobilities. [3-7] Recently two-dimensional layered group IV-VI semiconductors MX (M=Ge, Sn; X=S, Se) have been synthesized in the experiments.[22-25] SnSe monolayer is an analog of BP and each unit cell contains 4 atoms and 20 valence electrons.[26] Ferroelectricity and piezoelectricity were demonstrated in MX (M=Ge, Sn, Pb; X=S, Se, Te).[27-30] The structures of monolayer group IV-VI Semiconductors are similar to BP and each unit has the same ten valence electrons. Layered group IV-VI semiconductors have a much larger oxidation barrier compared to BP which yields the much stronger structural stability and they don't deteriorate in ambient conditions.[26]

Here we report the study of hexagonal honeycomb group IV-VI semiconductors in the layered formula. The hexagonal layered group IV-VI semiconductor is an analog of blue phosphorene but with a stronger structural stability. Moreover the electronic and magnetic properties can be modulated in a larger range. Valley effects, ferromagnetic states, Dirac fermions, and large spin-orbit splitting can be realized.

Computational methods

Theoretical calculations were performed by using the Quantum Espresso Package.[31] The Perdew–Burke–Ernzerhof (PBE) type of generalised gradient approximation exchange correlation functional was used.[32] Long-range van der Waals (vdW) dispersion corrections according to DFT-D3 procedure with Becke–Jonson damping were taken into account.[33-37] Moreover, calculations of using the PBE type of

generalised gradient approximation exchange correlation functional with non-local vdW dispersion corrections according to the vdW-DF2 procedure were also used to benchmark the calculations.[38-43] Furthermore, 500 eV was used as the cut-off energy of plane-wave basis set. The energy convergence criterion for the electronic wave function was set as 10^{-6} eV. The geometry optimization was considered to converge when the residual force on each atom was smaller than 1×10^{-3} eV/Å. A 20 Å thick vacuum layer normal to the plane was used to eliminate longitudinal interactions between the super cells. A 12×12×1 Monkhorst–Pack k-point mesh was used for the sampling of the Brillouin zone.

Result and Discussions

The optimized structures of monolayer and bilayer SnSe are shown in Fig. 1. The monolayer SnSe has a hexagonal honeycomb structure and the puckering between Sn and Se atoms is 1.56 Å as shown in Fig. 1a and Fig. 1d, respectively. The cohesive and formation energies of monolayer SnSe are respectively -7.68 and -0.72 eV per unit cell. The formation energy is defined as follows

$$\Delta H_f = E_{tot} - \sum_i n_i \mu_i \qquad (1)$$

where E_{tot} is the total energy of the group IV-VI semiconductors, μ_i denotes the chemical potential for species i of the crystalline bulks, and n_i is the corresponding number of atoms added to the supercell.

The cohesive energy was calculated by the following equation:

$$E_{coh} = E_{tot} - \sum_i n_i E_i \qquad (2)$$

where E_i is of the total energy of an isolated i-atom.

The Bilayer and monolayer exhibits drastically different physical properties for graphene.[44-45] The stacking order and twisting can modulate the electronic properties of 2D materials.[46-49] For the stacking of bilayer SnSe, six high-symmetry configurations are considered. The most stable configuration is shown in Fig. 1b and 1e and the total energy is 0.08~0.13 eV smaller than other configurations. We have also considered the bilayer SnSe in the similar configuration as that of In_2Se_2, but the relaxed structure can't form the two-dimensional In_2Se_2 type structures. For the

two-dimensional In_2Se_2 type structures, each In has one and three covalent bonds with the neighbouring In and Se atoms respectively.[3-7] Since In and Se have three and two valence electrons, thus In and Se atoms are fully paired in the two-dimensional In_2Se_2 type structures.

The Sn atoms on the top layer are in the hollow positions of the Se atoms on the bottom layer. We denote this hexagonal close-packed (HCP) stacking as AB configuration. The second most stable configuration is shown in Fig. 1c and 1f. The Sn atoms on the top layer are right above the Se atoms on the bottom layer and we denote this stacking as AA configuration. The total energy of AB configuration is of 0.01~0.06 eV, smaller than other configurations, obtained from the VDW-DF2 calculations. The vdW gaps between sheets for AB and AA configurations are 3.02 and 3.85 Å, respectively.

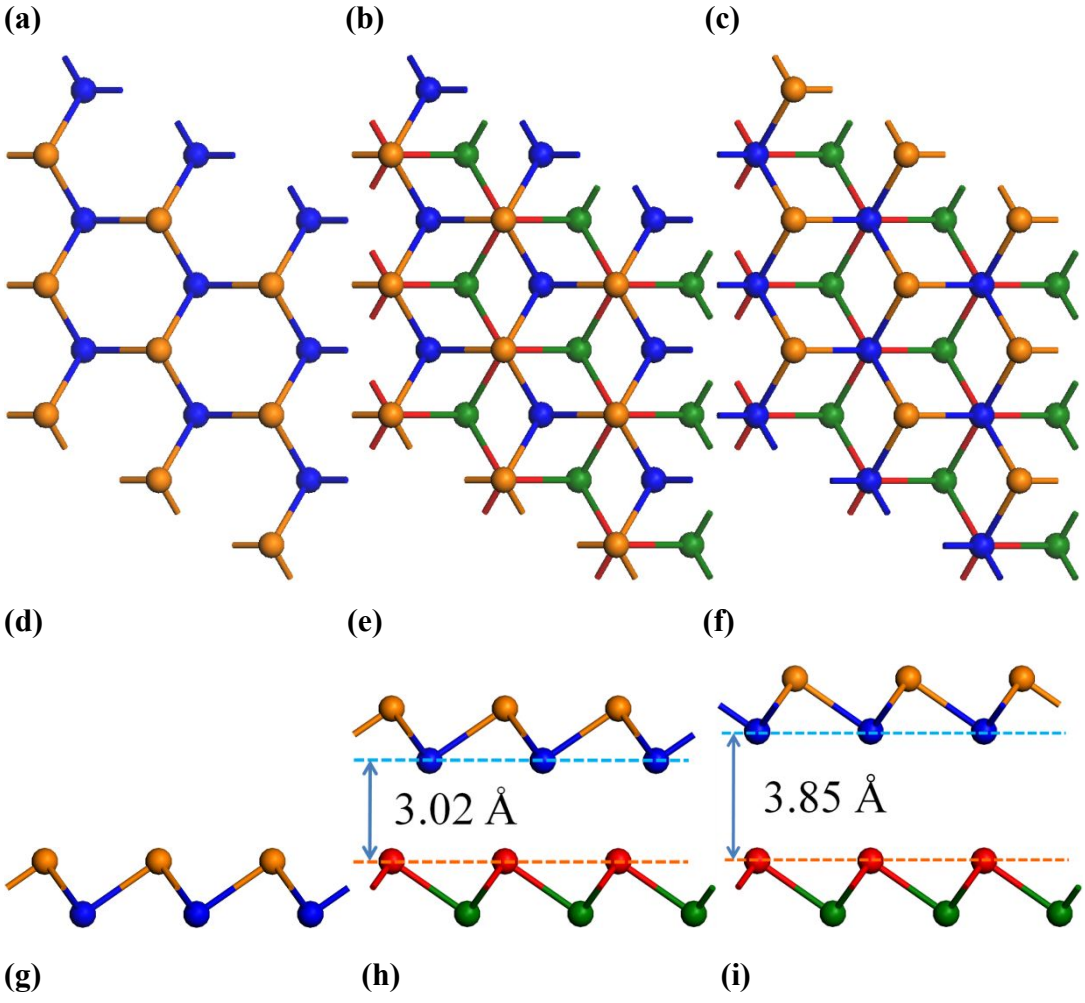

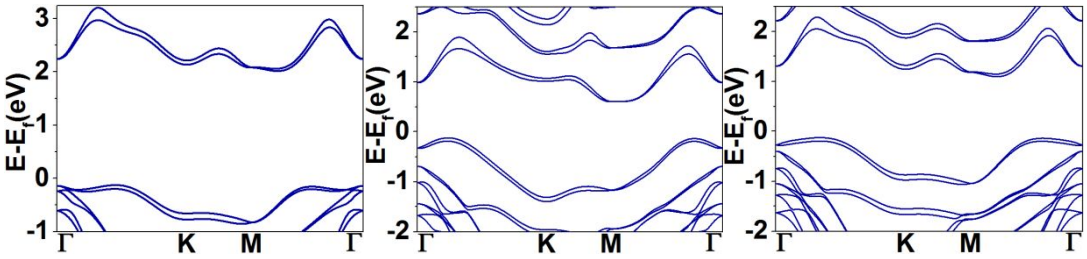

Fig. 1. Geometric structures of 3×3 SnSe unit cell and the band structures. Top views of (a) monolayer, (b) AB and (c) AA stacking bilayer. Side views of (d) monolayer, (e) AB and (f) AA stacking bilayer. Band structures of (g) monolayer, (h) AB and (i) AA bilayer. Orange (blue) and red (green) denote Se (Sn) atoms on the first and second layer, respectively. The vdW gap values are noted in (e) and (f).

The calculated band structures of SnSe monolayer, AB and AA stacking bilayer are shown in Fig. 1g, 1h and 1i respectively. The band gap of monolayer SnSe is 2.14 eV. The valence band maximum (VBM) and conduction band minimum (CBM) are along ΓK and MΓ respectively. The band structure of monolayer SnSe mimics that of blue phsophorene, but the SOC is stronger. The SOC induced energy splitting of VBM and CBM are 70 and 45 meV respectively. The interlayer coupling has modified significantly the band structure. The band gap has been reduced to 0.73 and 1.22 eV for AB and AA stacked SnSe bilayer. The interlayer coupling of AB stacking is stronger than that of AA stacking for SnSe bilayer. In the hexagonal crystal structures, the hexagonal close-packed (HCP) configurations were the most stable. The interlayer coupling and overlap of wave functions were the maximum in the HCP configurations, which resulted in the reduction of the total energy. Thus AB stacked SnSe bilayer is more stable than AA stacked SnSe bilayer. The band gap of AA stacking is 1.67 times that of AB stacking. The SOC energy splitting of VBM for SnSe bilayer is nearly the same as that of monolayer. Due to the absence of inversion symmetry, the valley-spin coupling effects exist.

The vdW layer-separations of various bilayer hexagonal honeycomb group IV-VI semiconductors of 2D hexagonal MX (M=Ge, Sn, Pb; X=S, Se, Te) are listed in table 1. The vdW layer-separations of HCP stacked AB bilayer are smaller than these of

AA stacked bilayer. Their averaged vdW gaps of AB and AA bilayers are 2.89 and 3.77 Å, respectively for 2D hexagonal MX (M=Ge, Sn, Pb; X=S, Se, Te). The 0.88 Å vdW gap difference indicates the large difference of interlayer coupling strength due to the different stacking venues. The band gaps of monolayer and bilayer hexagonal honeycomb group IV-VI semiconductors are listed in table 2. We are noted that the theoretical and computational 2D Materials Databases from first-principles calculations have been produced.[50-52] The calculated results regarding monolayer are in good agreement with Computational 2D Materials Database.[50] The general trend is that the heavier the atoms are, the smaller the band gaps will be. The averaged band gap of monolayer MX is 1.87 eV. Monolayer PbSe and PbTe are direct band gap semiconductors and all others are indirect band gap semiconductors. The averaged band gap of AB bilayer is only 30.48% of that of monolayer. Thus interlayer coupling can greatly change the band gap. The averaged band gap of AB bilayer is 62.63% of that of AA stacking. The interlayer coupling strength of 2D materials can be effectively tuned by the hydrostatic pressures.[53-56]

Table 1. VdW gaps (Å) of bilayer hexagonal MX.

	GeS	GeSe	GeTe	SnS	SnSe	SnTe	PbS	PbSe	PbTe
AB bilayer	3.07	2.85	2.72	3.06	3.02	2.93	2.78	2.79	2.84
AA bilayer	3.84	3.69	3.83	3.77	3.85	3.88	3.62	3.70	3.77

Table 2. Band gaps (eV) of monolayer and bilayer hexagonal MX.

	GeS	GeSe	GeTe	SnS	SnSe	SnTe	PbS	PbSe	PbTe
Monolayer	2.43	2.37	1.46	2.27	2.14	1.55	1.91	1.64	1.07
AB bilayer	1.19	0.79	0.37	0.85	0.73	0.41	0.34	0.30	0.13
AA bilayer	1.61	1.31	0.95	1.26	1.22	0.88	0.351	0.37	0.20

2D hexagonal MX semiconductors are functionalized by halogens and oxygen that can tune the electronic and magnetic properties. The calculated structures of F functionalized 2D MX are shown in Fig. 2. F atoms are chemisorbed on Ge and Sn

atoms. The adsorption energy is calculated by

$$E_{ad} = -(E_{total} - E_{substrate} - nE_{adatom}) / n \qquad (3)$$

where E_{total} is the total energy of the whole system (MX substrate plus adatoms); $E_{substrate}$ is the total energy of the pristine MX substrate; E_{adatom} is the total energy of an isolated adatom. The adsorption energy is positive when the adsorption is exothermic. The larger adsorption energy indicates a stronger interaction between substrate and adatoms and a more stable system. The adsorption energy is 3.88, 4.01 and 4.06 eV for F adsorption on GeSe, SnS and SnSe monolayer, respectively.

The spin density distribution is shown in Figs. 2g, 2h and 2i. The net spin is mainly localized on the F-adsorbed group IV and three neighboring group VI atoms. The magnetization is projected to atoms. For the F adsorbed GeSe, the Ge and one neighboring Se have the magnetic moment of 0.29 and 0.37 μB, respectively. The other two neignboring Se atoms have the magnetic moment of 0.09 μB and the F atom has the magnetic moment of 0.13 μB. For F adsorberd SnSe, the Sn has the largest magnetic moment of 0.39 μB and the neighboring Se atoms have the total magnetic moment of 0.51 μB. The F adatom has 0.09 uB. For F adsorberd SnS, the Sn has the magnetic moment of 0.43 μB and the three neighboring S atoms have the total magnetic moment of 0.46 μB. The F atom has 0.08 μB magnetic moment. Though the detailed atomic magnetization distribution is different, the total magnetic moment is the same. Each F adatom will result in the total magnetic moment of 1 μB. The atomic-decomposed magnetic moment is shown in Table 3. These five atoms compose 97 percents of the total magnetic moment.

The SPDOS for F adsorbed MX monolayer is shown in Figs. 2j, 2k and 2l. F adatom has strong hybridization with the substrate which results in the band gap states. Accordingly the band gap of MX monolayer is reduced and strong spin-polarization is generated. In the vicinity of Fermi level, the spin up and down states are staggered. Both the band gaps of spin up and down states are reduced due to the F adsorption. For F adsorbed GeSe, the band gaps of spin up and down states are 1.75 and 1.15 eV, respectively. For F adsorbed SnS, the band gaps of spin up and down states are 2.02

and 0.91 eV, respectively. For F adsorbed SnSe, the band gaps of spin up and down states are 1.93 and 0.75 eV, respectively. Compared to the pristine monolayer, the band gaps have been reduced. Especially, the band gap of spin down state has been reduced to less than half that of pristine monolayer.

Table 3. Atomic-decomposed magnetic moment (μB) of the atoms for the F functionalized MX.

	1	2	3	4	5
GeSe	0.29	0.13	0.37	0.09	0.09
SnS	0.43	0.10	0.30	0.08	0.08
SnSe	0.39	0.09	0.33	0.09	0.09

.

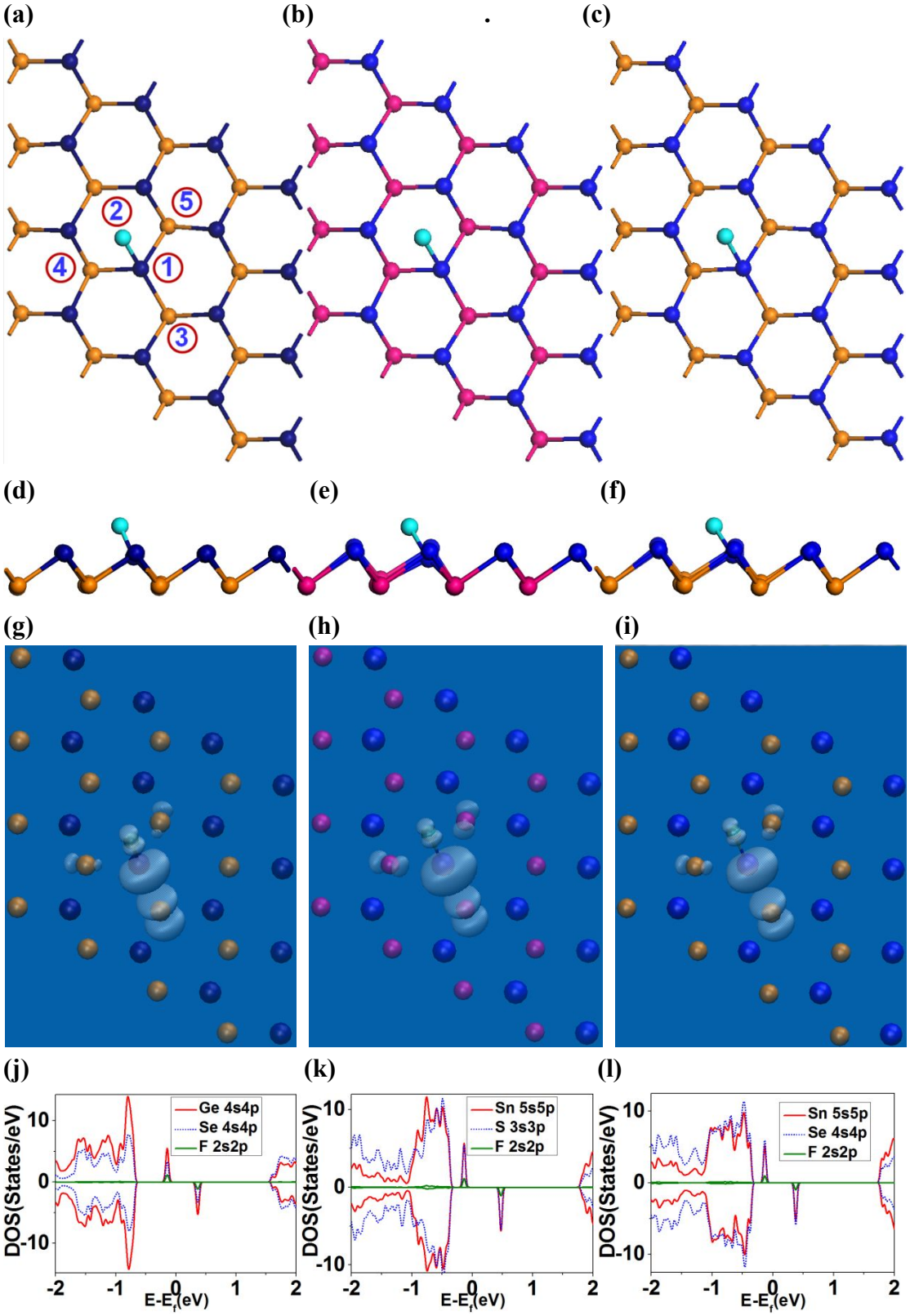

Fig. 2. Optimized structures and electronic structures of F functionalized 2D MX. Top views of F doped (a) GeSe, (b) SnS and (c) SnSe; side views of F doped (d) GeSe, (e) SnS and (f) SnSe. Isosurfaces of the spin density distribution of F doped (g) GeSe, (h) SnS and (i) SnSe. SPDOS of F doped (j) GeSe, (k) SnS and (l) SnSe.

The increase of F concentration further tunes the electronic and magnetic properties of MX. Here we define the full monolayer coverage as every Sn on the top layer absorbing one F. The optimized structure and the distribution of net spin of one monolayer coverage of F atoms are shown in Fig. 3a and 3b respectively. Each F adatom has a chemical bond with Sn. All atoms are magnetic. Sn, Se and F atoms have the magnetic moments of 0.37, 0.45 and 0.18 μB, respectively. The side view of optimized structure and band structure w/ SOC are shown in Fig. 3c and 3d, respectively. There are eight bands in the forbidden gap of SnS indicating the insulator-to-metal transition. The existence of magnetization has broken the time-reversal-symmetry. The spin up and down bands have the SOC energy split of 0.23 eV at Γ in the vicinity of Fermi level.

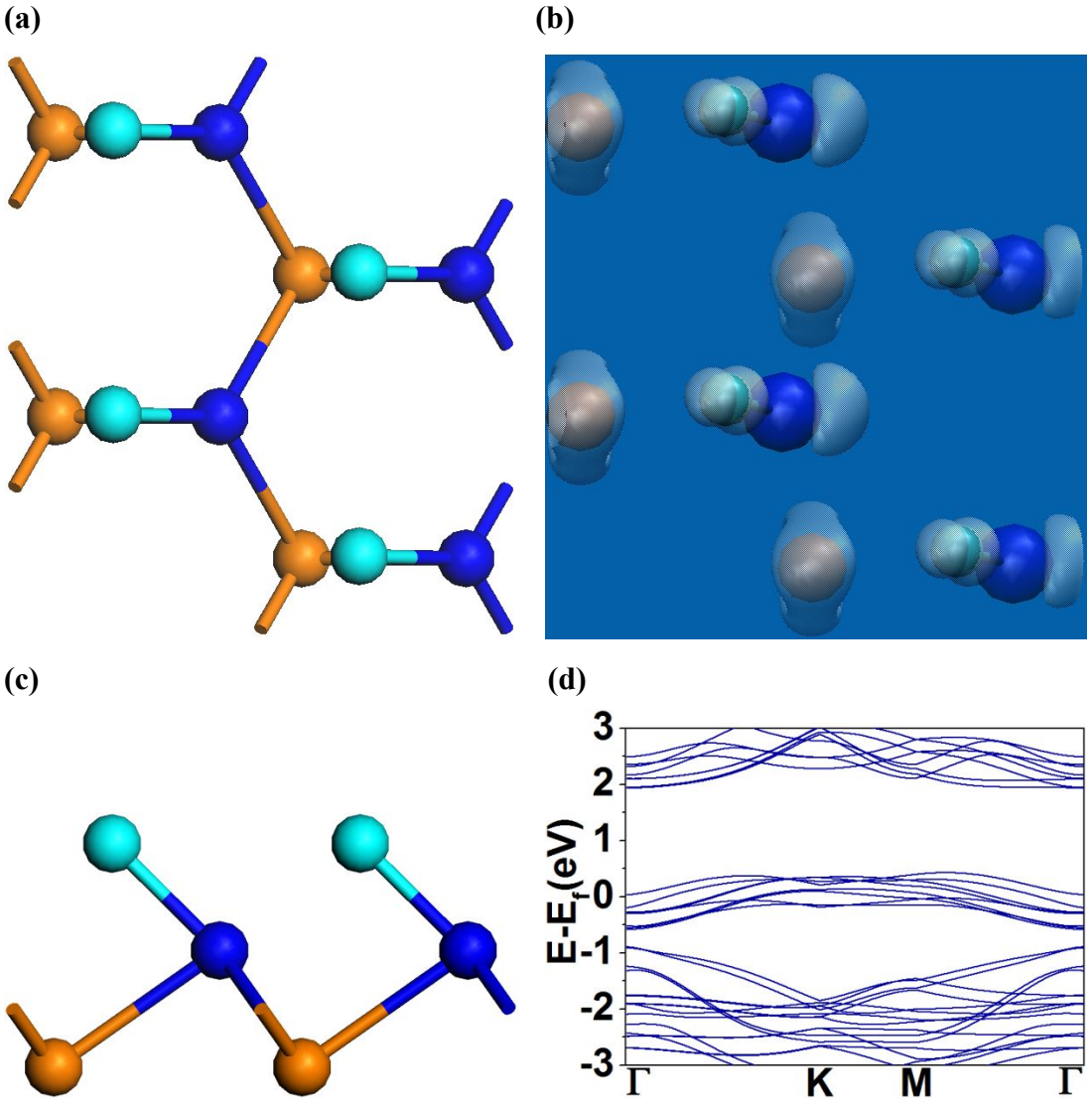

Fig. 3. Optimized structures and electronic structures of F functionalized SnSe. (a) Top view, (b) net spin density distribution, (c) side view and (d) band structure of F doped SnSe.

The magnetic exchange coupling between magnetic atoms was investigated. The total energy difference between the ferromagnetic (FM) and antiferromagnetic (AFM) states is defined as follows:

$$\Delta E = E_{AF} - E_F \quad (4)$$

The magnetic exchange interactions between the magnetic atoms in the Heisenberg model are expressed as follows:

$$H = -\sum_{i \neq j} J_{ij} S_i \cdot S_j \quad (5)$$

where J_{ij} denotes the magnetic exchange coupling between two nearest-neighbouring magnetic atoms and S_i represent the spin of magnetic atom i. The spin of the atom is given by $S = (N_\uparrow - N_\downarrow)/2$;[57-58] here, $N_\uparrow$ and $N_\downarrow$ denote the number of spin-up and spin-down electrons, respectively. The Curie temperature (T_C) as estimated by using the mean field method was as follows: [57-60]

$$T_C = \frac{2S(S+1)}{3k_B} \frac{1}{N} \sum_{i \neq j} J_{ij} \quad (6)$$

where N is the number of magnetic atoms. The results of T_c calculated from mean field solutions of Heisenberg model are usually in fair agreement with experimental results.[58] Since the spin fluctuation effects are neglected, the calculated *Tc* is above the experimental result and the error is around 30~40 percents. The ΔE=69.3 meV was found so that ferromagnetic state is more stable than the antiferromagnetic one. The corresponding T_C is 199.8 K. The ΔE was 8.6 and 64.3 meV for F monolayer doped GeSe and SnS respectively, which implies that the magnetic coupling is weaker than that of F doped SnSe. The T_C is 24.8 and 185.4 K for F monolayer adsorbed GeSe and SnS respectively. One F adatom can induce one μB in GeSe, SnS and SnSe. However the F monolayer adsorbed GeS doesn't exhibit any magnetism. All F functionalized PbX (X=S, Se, Te) don't exhibit magnetism. Similar ferromagnetism has been found in hydrogen functionalized graphene monlayer.[59]

The concentration of halogen atoms is further increased. Both the top and bottom surfaces are functionalized with halogen atoms. The optimized structures of Cl atoms functionalized SnSe are shown in Fig. 4a and 4b. There are four atoms in linear like structure in each unit cell. The band structure of Cl atoms functionalized SnSe is shown in Fig. 4c. The band gap is 1.452 eV. Cl functionalization results in indirect to direct band gap transition for SnSe. Both the CBM and VBM move to the K point and they have the spin energy splitting of 29 meV. The band structure in the vicinity of Fermi level obeys the relativistic band dispersion

$$E = E_{Apex} \pm \sqrt{m^2 v_F{}^4 + v_F{}^2 \hbar^2 k^2} \qquad (7)$$

Where v_F is the Fermi velocity, k is the wave vector, and m is the rest effective mass. According to our fitting, the Fermi velocity is around 8.53×10^5 and 7.48×10^5m/s for electron and hole carriers respectively, and the rest mass is zero.

The band gap is 1.113 eV at *K* for Br functionalized SnSe as shown in Fig. 4d. The indirect band gap is 1.086 eV. The SOC energy split is 46 and 71 meV for CBM and VBM respectively. The band structure obeys the relativistic band dispersion as E.q. (7) in the vicinity of band gap at *K*. The Fermi velocity of electron carrier is around 9.35×10^5 and 6.23×10^5 m/s for electron and hole carriers respectively in the vicinity of K and the rest mass is zero. The band structure of -OH functinalized SnSe is shown in Fig. 4e. It has an indirect band gap of 2.078 eV. The VBM has a SOC energy split of 47 meV. The top valence band resembles the relativistic band dispersion as E.q. (7) in the vicinity of *K*. The Fermi velocity of electron carrier is around 1.35×10^6 m/s, which is above that of graphene. The rest mass is zero.

F atoms are used to functionalize both the top and bottom surfaces of SnSe. The optimized structure is similar to the Cl functionalized SnSe. The indirect band gap is 2.093 eV. Both CBM and VBM are not at *K*. The top valence band resembles the relativistic band dispersion as E.q. (7) in the vicinity of *K*. The Fermi velocity of electron carrier is around 1.25×10^6 m/s, which is above that of graphene.

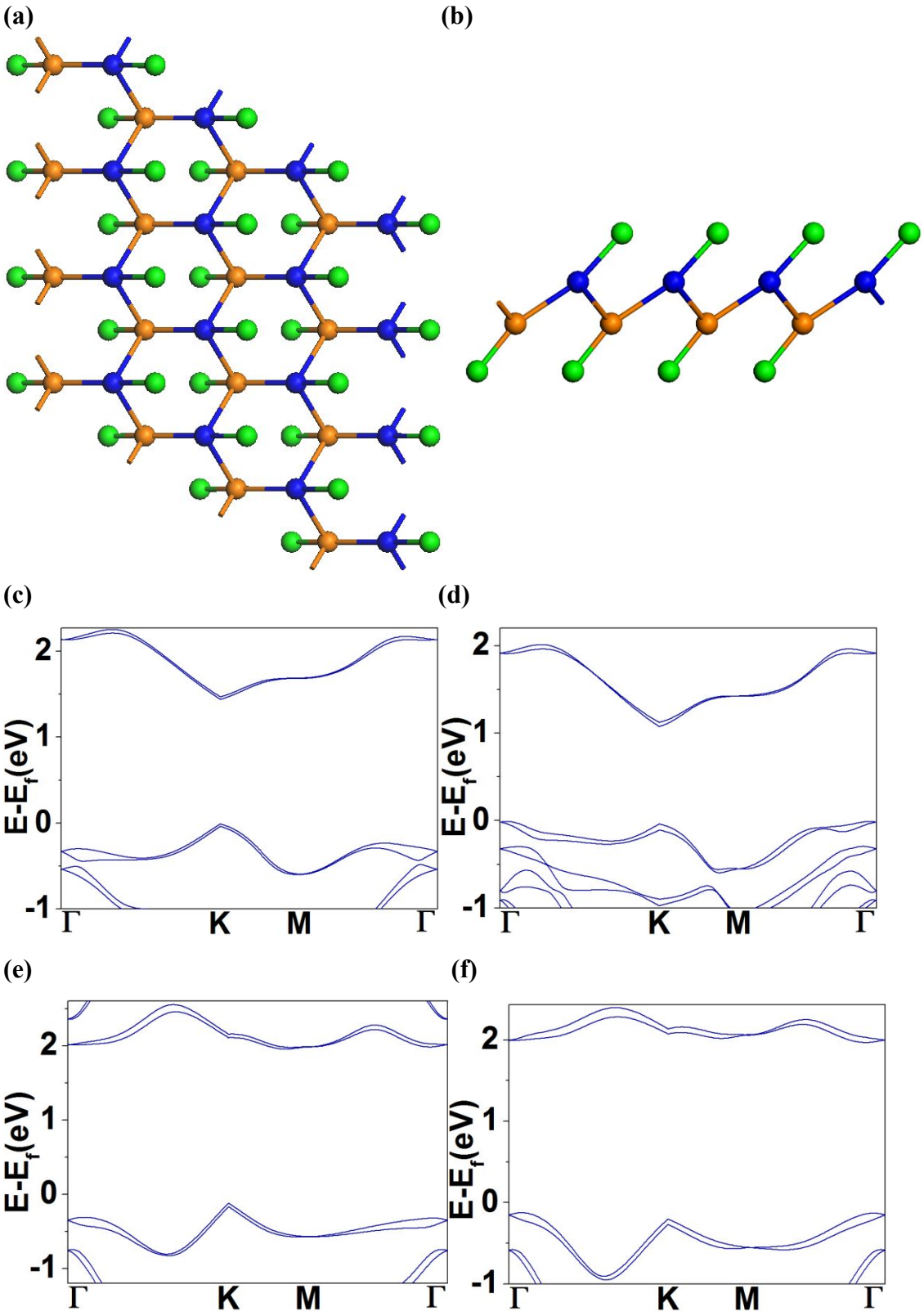

Fig. 4. Optimized structures and electronic structures of F functionalized 2D MX. (a) Top and (b) side views of F doped SnSe. Band structures of (c) Cl, (d) Br, (e) OH and (f) F dopoed SnSe.

Conclusions

The hexagonal 2D MX semiconductors are predicted and the unusual physical

properties are revealed. The interlayer coupling can reduce the band gap and stacking order has the strong influence. The electronic properties can be modulated by atomic functionalization. Semiconductor-metal-semiconductor transitions are realized. Halogens adsorption can induce high T_C ferromagnetism. Gapped Dirac Fermions with ultra zero masses are developed. The Fermi velocity can be above that of graphene.

Acknowledgements

We thank Prof. X. C. Xie and Prof. J. Feng of Peking University and Prof Y. G. Yao of Beijing Institute of Technology for helpful discussions. This work was supported by the NSFC (11774296, 11734012, 61901274, 11574217, 11574218 and 11504241), NSF of Guangdong (2018A0303130311, 2016A030313059, 2020A1515010467), Science and Technology plan project of Guangdong (2017A010101018), Science and Technology plan project of Shenzhen (KQJSCX20180328093801773, JCYJ20180305124540632 and JCYJ20190808121405740, JCYJ20190808145207437, JCYJ20190808141818890), the Hong Kong RGC (16301619 and 16300117). B.I.Y. was supported by the Army Research Office (W911NF-16-1-0255), the Office of Naval Research (N00014-15-1-2372), US Department of Energy (DE-SC0012547) and by the R. Welch Foundation (C-1590).

References

[1] A. H. Castro Neto, F. Guinea, N. M. R.Peres, K. S. Novoselov, and A. K. Geim, The electronic properties of graphene. *Rev. Mod. Phys.* 2009, **81**, 109.

[2] K. F. Mak, K. L. McGill, J. Park, P. L. McEuen, The valley Hall effect in MoS_2 transistors. *Science* 2014, **344**, 6191.

[3] V. Z´olyomi, N. D. Drummond, and V. I. Fal'ko, Electrons and phonons in single layers of hexagonal indium chalcogenides from ab initio calculations, *Phys. Rev.B* 2014, **89**, 205416.

[4] S. J. Magorrian, V. Z´olyomi, and V. I. Fal'ko, Electronic and optical properties of two-dimensional InSe from a DFT-parametrized tight-binding model, *Phys. Rev.B* 2016, 94, 245431.

[5] V. Z´olyomi, N. D. Drummond, and V. I. Fal'ko, Band structure and optical transitions in atomic layers of hexagonal gallium chalcogenides, *Phys. Rev.B* 2013, 87, 195403.

[6] D. A. Bandurin, A. V. Tyurnina, G. L. Yu, A. Mishchenko, V. Zólyomi, S. V. Morozov, R. K. Kumar, R. V. Gorbachev, Z. R. Kudrynskyi, S. Pezzini, Z. D. Kovalyuk, U. Zeitler, K. S. Novoselov, A. Patanè, L. Eaves, I. V. Grigorieva, V. I. Fal'ko, A. K. Geim and Yang Cao, High electron mobility, quantum Hall effect and anomalous optical response in atomically thin InSe, *Nat. Nanotech.* 2017, **12**, 223.

[7] A. Y. Gao, J. W. Lai, Y. J. Wang, Z. Zhu, J. W. Zeng, G. L. Yu, N. Z. Wang, W. C. Chen, T. J. Cao, W. D. Hu, D. Sun, X. H. Chen, F. Miao, Y. Shi and X. M. Wang, Observation of ballistic avalanche phenomena in nanoscale vertical InSe/BP heterostructures, *Nat. Nanotech.* 2019, **14**, 217.

[8] F. F. Zhu, W. J. Chen, Y. Xu, C. L. Gao, D. D. Guan, C. H. Liu, D. Qian, S. C. Zhang, J. F. Jia, Epitaxial growth of two-dimensional stanene. *Nature Materials* 2015, **14**, 1020.

[9] A. Molle, J. Goldberger, M. Houssa, Y. Xu, S. C. Zhang, D. Akinwande, Buckled Two-dimensional Xene sheets. *Nature Mater.* 2017, **16**, 163.

[10] C. Gong, L. Li, Z. L. Li, H. W. Ji, A. Stern, Y. Xia, T. Cao, W. Bao, C. Z. Wang, Y. Wang, Z. Q. Qiu, R. J. Cava, S. G. Louie, J. Xia, X. Zhang, Discovery of intrinsic ferromagnetism in two-dimensional van der Waals crystals. *Nature* 2017, **546**, 265.

[11] B. Huang, G. Clark, E. Navarro-Moratalla, D. R. Klein, R. Cheng, K. L. Seyler, D, Zhong, E. S. M. A. McGuire, D. H. Cobden, W. Yao, D. Xiao, P. Jarillo-Herrero, X. D. Xu, Layer-dependent ferromagnetism in a van der Waals crystal down to the monolayer limit. *Nature.* 2017, **546**, 270.

[12] T. C, Song, X. H. Cai, M. W. Y. Tu, X. O. Zhang, B. Huang, N. P. Wilson, K, L. Seyler, L. Zhu, T. Taniguchi, K. Watanabe, M. A. McGuire, D. H. Cobden, D. Xiao, W. Yao, X. D. Xu, Giant tunneling magnetoresistance in spin-filter van der Waals heterostructures. *Science*. 2018,**360**,6394.

[13] J. S. Qiao, X. H. Kong, Z. X. Hu, F. Yang W. Ji, High-mobility transport anisotropy and linear dichroism in few-layer black phosphorus. *Nature*

Communications 2014, **5**, 4475.

[14] X. M. Wang, A. M. Jones, K. L. Seyler, V. Tran, Y. Jia, H. Zhao, H. Wang, L. Yang, X. Xu, F. Xia, Highly anisotropic and robust excitons in monolayer black phosphorus. *Nature Nanotechnology.* 2015,**10**, 517–521.

[15] L.K. Li, Y. J. Yu, G. J. Ye, Q. q. Ge, X. D. Ou, H. Wu, D. L. Feng, X. H. Chen, Y. B. Zhang, Black Phosphorus Field-effect Transistors. *Nat. Nanotechnol.* 2014,**10**, 327-377.

[16] H. Liu, A. T. Neal, Z. Zhu, Z. Luo, X. F. Xu, D. Tomanek, P. D. Ye, Phosphorene: An Unexplored 2D Semiconductor with a High Hole Mobility. *ACS Nano* 2014, **8**, 4033−4041.

[17] J. L. Zhang, S. T. Zhao, C. Han, Z. Z. Wang, S. Zhong, S. Sun, R. Guo, X. Zhou, C. D. Gu, K. D. Yuan, Z. Y. Li, W. Chen, The Synergic Effect of Atomic Hydrogen Adsorption and Catalyst Spreading on Ge Nanowire Growth Orientation and Kinking. *Nano Lett.* 2016 ,**8**,16.

[18] C. D. Gu, S. T. Zhao, J. L. Zhang, S. Sun, K. D. Yuan, Z. H. Hu, C. Han, Z. R. Ma, Li. Wang, F. W. Huo, W. Huang, Z. Y. Li, W. Chen, Growth of Quasi-Free-Standing Single-Layer Blue Phosphorus on Tellurium Monolayer Functionalized Au(111). *ACS Nano,* 2017, **5**,11.

[19] J. C. Zhuang, C. Liu, Q. Gao, Y. N. Liu, H. F. Feng, X. Xu, J. O. Wang, J. J. Zhao, S. X. Dou, Z. P. Hu, Y. Du, Band Gap Modulated by Electronic Superlattice in Blue Phosphorene. *ACS Nano* 2018, **12**, 5059-5065.

[20] J. P. Xu, J. Q. Zhang, H. Tian, H. Xu, W. K. Ho, M. H. Xie, One-dimensional phosphorus chain and two-dimensional blue phosphorene grown on Au (111) by molecular-beam epitaxy, *Phys. Rev. Mater.* 2017, **1**, 6.

[21] Z. Zhu, D. Tománek, Semiconducting Layered Blue Phosphorus: A Computational Study. *Phys. Rev. Lett.*, 2014, **112**, 176802.

[22] L. Li, Z. Chen, Y. Hu, X. W. Wang, T. Zhang, W. Chen, Q. B. Wang, Single-Layer Single-Crystalline SnSe Nanosheets. *J. Am. Chem. Soc*. 2013, 135,4.

[23] D. J. Xue, S. C. Liu, C. M. Dai, S. Y. Chen, C. He, L. Zhao, J. S. Hu, L. J. Wan, GeSe Thin-Film Solar Cells Fabricated by Self-Regulated Rapid Thermal Sublimation.

J. Am. Chem. Soc. 2017, **139**, 2.

[24] A. J. Biacchi, D. D. Vaughn II, R. E. Schaak, Synthesis and Crystallographic Analysis of Shape-Controlled SnS Nanocrystal Photocatalysts: Evidence for a Pseudotetragonal Structural Modification. *J. Am. Chem. Soc.* 2013, **135**, 31.

[25] F. O. v. Rohr, H. W. Ji, F. A. Cevallos, T. Gao, N. P. Ong, R. Cava, High-Pressure Synthesis and Characterization of β GeSe A Six-Membered-Ring Semiconductor in an Uncommon Boat Conformation. J. *J. Am. Chem. Soc.* 2017, **139**, 7.

[26] V. L. Deringer, R. P. Stoffel, R. Dronskowski, Vibrational and thermodynamic properties of GeSe in the quasiharmonic approximation. *Phys. Rev. B* 2014, **89**, 094303.

[27] L.-D. Zhao, S.-H. Lo, Y. Zhang, H. Sun, G. Tan, C. Uher, C. Wolverton, V. P. Dravid, M. G. Kanatzidis, Ultralow Thermal Conductivity and High Thermoelectric Figure of Merit in SnSe Crystals. Nature2014, **508**, 373–377.

[28] I. Pletikosić, F. v. Rohr, P. Pervan, P. K. Das, I. Vobornik, R. J. Cava, T. Valla, Band Structure of the IV-VI Black Phosphorus Analog and Thermoelectric SnSe. *Phys. Rev. Lett.* 2018,**120**, 156403.

[29] R. Fei, W. Kang, L. Yang, Ferroelectricity and Phase Transitions in Monolayer Group-IV Monochalcogenides. *Phys. Rev. Lett*. 2016, **117**, 097601.

[30] L. C. Gomes, A. Carvalho, A. H. C. Neto, Enhanced piezoelectricity and modified dielectric screening of two-dimensional group-IV Monochalcogenides. *Phys. Rev. B* 2015,**92**, 214103.

[31] P. Giannozzi, S. Baroni, N. Bonini, M. Calandra, R. Car, C. Cavazzoni, D. Ceresoli, G. L. Chiarotti, M. Cococcioni, I. Dabo, A. Dal Corso, S. de Gironcoli, S. Fabris, G. Fratesi, R. Gebauer, U. Gerstmann, C. Gougoussis, A. Kokalj, M. Lazzeri, L. Martin−Samos, N. Marzari, F. Mauri, R. Mazzarello, S. Paolini, A. Pasquarello, L. Paulatto, C. Sbraccia, S. Scandolo, G. Sclauzero, A. P. Seitsonen, A. Smogunov, P. Umari, R. M. Wentzcovitch, QUANTUM ESPRESSO: A modular and open-source software project for quantum simulations of materials, *J. Phys.: Condens Matter.* 2009, **21**, 395502.

[32] J. P. Perdew, K. Burke, M. Ernzerhof, Generalized Gradient Approximation Made Simple. *Phys. Rev. Lett.* 1996, **77**, 3865−3868.

[33] S. *J.* Grimme, Semiempirical GGA-type density functional constructed with a long-range dispersion correction. *Comput. Chem.* 2006, **27**, 1787−1799.

[34] S. Grimme, J. Antony, S. Ehrlich, H. Krieg, A consistent and accurate ab initio parametrization of density functional dispersion correction (DFT-D) for the 94 elements. *J. Chem. Phys.* 2010, **132**, 154104.

[35] S. Grimme, S. Ehrlich, L. Goerigk, Benchmark assessment of the accuracy of several van der Waals density functional. *J. Comput. Chem.* 2011, **32**, 1456−1465.

[36] A. Tkatchenko, R. A. DiStasio, R. Car, M. Scheffler, Accurate and Efficient Method for Many-Body van der Waals Interactions. *Phys. Rev. Lett.* 2012, **108**, 236402.

[37] A. Tkatchenko, M. Scheffler, Accurate Molecular Van Der Waals Interactions from Ground-State Electron Density and Free-Atom Reference Data. *Phys. Rev. Lett.* 2009, **102**, 073005.

[38] M. Dion, H. Rydberg, E. Schroder, D. C. Langreth, B. I. Lundqvist, Van der Waals Density Functional Theory (vdW-DF) Basis and Applications. *Phys. Rev. Lett.* 2004, **92**, 246410.

[39] K. Lee, E. D. Murray, Z. Kong, L. B. I. Lundqvist, D. C. Langreth, Higher-accuracy van der Waals density functional. *Phys. Rev. B: Condens. Matter Mater. Phys.* 2010, ***82***, 081101.

[40] G. Roman−Perez, J. M. Soler, Efficient Implementation of a van der Waals Density Functional: Application to Double-Wall Carbon Nanotubes. *Phys. Rev. Lett.* 2009, **103**, 096102.

[41] J. Klimes, D. R. Bowler, A. Michaelides, Chemical accuracy for the van der Waals density functional. *J. Phys.: Condens. Matter.* 2010, ***22***, 022201.

[42] J. Klimes, D. R. Bowler, A. Michaelides, Van der Waals density functionals applied to solids. *Phys. Rev. B: Condens. Matter Mater. Phys.* 2011, ***83***, 195131.

[43] T. Thonhauser, V. R. Cooper, S. Li, A. Puzder, P. Hyldgaard, D. C. Langreth, Van der Waals density functional: Self-consistent potential and the nature of the van

der Waals bond. *Phys. Rev. B* 2007, ***76***, 125112.

[44] E. McCann and V. I. Fal'ko, Landau-Level Degeneracy and Quantum Hall Effect in a Graphite Bilayer, *Phys. Rev. Lett.* 2006, **96**, 086805.

[45] K. S. Novoselov, E. McCann, S. V. Morozov, V. I. Fal'ko, M. I. Katsnelson, U. Zeitler, D. Jiang, F. Schedin and A. K. Geim, Unconventional quantum Hall effect and Berry's phase of 2π in bilayer graphene, *Nat. Phys.* 2006, **2**, 177.

[46] S. Y. Lei, H. Wang, L. Huang, Y. Y. Sun, S. B. Zhang, Stacking Fault Enriching the Electronic and Transport Properties of Few-Layer Phosphorenes and Black Phosphorus. *Nano Lett.* 2016, **16**, 2.

[47] L. Huder, A. Artaud, T. L. Quang, G. T. d. Laissardière, A. G. M. Jansen, G. Lapertot, C. Chapelier, V. T. Renard, Electronic Spectrum of Twisted Graphene Layers under Heterostrain. *Phys. Rev. Lett*. 2018, 120, 15.

[48] L. A. Gonzalez-Arraga, J. L. Lado, F. Guinea, P. S. Jose, Electrically Controllable Magnetism in Twisted Bilayer Graphene. *Phys. Rev. Lett.* 2017,**119**, 107201.

[49] Y. Cao, J. Y. Luo, V. Fatemi, S. Fang, J. D. Sanchez-Yamagishi, K. Watanabe, T. Taniguchi, E. Kaxiras, P. Jarillo-Herrero, Superlattice-Induced Insulating States and Valley-Protected Orbits in Twisted Bilayer Graphene. *Phys. Rev. Lett* 2016, **117**, 116804.

[50] S. Haastrup, M. Strange, M. Pandey, T. Deilmann, P. S. Schmidt, N. F. Hinsche, M. N. Gjerding, D. Torelli, P. M. Larsen, A. C. Riis-Jensen, J. Gath, K. W. Jacobsen, J. Jørgen Mortensen, T. Olsen, K. S. Thygesen, The Computational 2D Materials Database: high-throughput modeling and discovery of atomically thin crystals. 2D Mater. 2018, **5**, 042002.

[51] N. Mounet, M. Gibertini, P. Schwaller, D. Campi, A. Merkys, A. Marrazzo, T. Sohier, I. E. Castelli, A. Cepellotti, G. Pizzi, N. Marzari, Two-dimensional materials from high-throughput computational exfoliation of experimentally known compounds. Nat. Nanotechnol. 2018, **13**,246–252.

[52] K. Choudhary, I. Kalish, R. Beams, F. Tavazza, High-throughput Identification and Characterization of Two-dimensional Materials using Density functional theory,

Scientific Reports 2017, **7**, 5179.

[53] Y. B. Chen, F. Ke, P. H. Ci, C. H. Ko, T. Park, S. Saremi, H. L. Liu, Y. Lee J. Suh, L. W. Martin, J. W. Ager, B. Chen, J. Q. Wu, Pressurizing Field-Effect Transistors of Few-Layer MoS2 in a Diamond Anvil Cell. *Nano Lett.*, 2017, **17**,1.

[54] A. P. Nayak, T. Pandey, D. Voiry, J. Liu, S. T. Moran, A. Sharma, C. Tan, C. H. Chen, L. J. Li, M. Chhowalla, J. F. Lin, A. K. Singh, D. Akinwande, Pressure-Dependent Optical and Vibrational Properties of Monolayer Molybdenum Disulfide. *Nano Lett.*2015,**15**,1.

[55] Y. Q. Zhu, T. Sekine, Y. H. Li, M. W. Fay, Y. M. Zhao, C. H. P. Poa, W. X. Wang, M. J. Roe, P. D. Brown, N. Fleischer, R. Tenne, Shock-Absorbing and Failure Mechanisms of WS2 and MoS2 Nanoparticles with Fullerene-like Structures under Shock Wave Pressure. *J. Am. Chem. Soc.*, 2005, **127**,46.

[56] M. Yankowitz, J. Jung, E. Laksono, N. Leconte, B. L. Chittari, K. Watanabe, T. Taniguchi, S. Adam, D. Graf, C. R. Dean, Dynamic band-structure tuning of graphene moiré superlattices with pressure. *Nature* 2018,**557**, 7705.

[57] X. Q. Tian, X. R. Wang, Y. D. Wei, L. Liu, Z. R. Gong, J. Gu, Y. Du, B. I. Yakobson, Highly Tunable Electronic Structures of Phosphorene/Carbon Nanotube Heterostructures Through External Electric Field and Atomic Intercalation. *Nano Lett.* 2017, **17**, 12.

[58] X. Q. Tian, L. Liu, Y. Du, J. Gu, J. B. Xu, B. I. Yakobson, Effects of 3d transition-metal doping on electronic and magnetic properties of MoS_2 nanoribbons. *Phys. Chem. Chem. Phys.* 2015, **17**, 1831−1836.

[59] J. Zhou, Q. Wang, Q. Sun, X. S. Chen, Y. Kawazoe, and P. Jena, Ferromagnetism in Semihydrogenated Graphene Sheet, *Nano Letters* 2009, **9**, 3867.

[60] P. Mohn, Magnetism in the Solid State: An Introduction, Springer-Verlag, Berlin Heidelberg, 2006.

TOC graphic

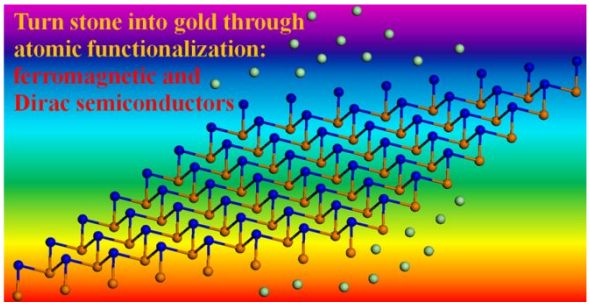
Turn stone into gold through
atomic functionalization:
ferromagnetic and
Dirac semiconductors